Journal of Interfaces, Thin films, and Low dimensional systems 7 (2) Winter and Spring (2024) 747-755

Fractal analysis of ballistic deposition model with power-law distributed noise

Scientific research paper

Masoumeh Rahimi[1*], Sakineh Hosseinabadi[2], Amir Ali Masoudi[3], Laleh Farhang Matin[1]

[1]*Department of Physics, North Tehran Branch, Islamic Azad University, Tehran, Iran*

[2]*Department of Physics, East Tehran Branch, Islamic Azad University, Tehran, Iran*

[3]*Department of Condensed Matter Physics, Faculty of Physics, Alzahra University, Tehran, Iran*

ARTICLE INFO

Article history:
Received 10 October 2023
Revised 26 November 2023
Accepted 4 December 2023
Available online 22 March 2024

Keywords
Ballistic deposition model
Power-law noise
Contour loops
Fractal dimension

ABSTRACT

The ballistic deposition model with power-law distributed noise (BD-PLN) has been simulated and investigated. Analysis of scaling exponents and statistical features seems essential in understanding the mechanism of noise in the phenomena. In the BD-PLN model, heterogeneous particles with rod-like shapes are deposited during growth time and lead to the forming of porous structures. By using the Hoshen-Kopelman algorithm, porous structures are converted to contour loops, and the fractal properties of the loops are considered. The fractal dimension of each loop, D_f, the fractal dimension of the contour set, d, the generalized dimensions, D_q, and the mass function, τ_q are calculated. The fractal dimension, d, increases as $d = a + b\mu^c$ versus μ exponent, and remains constant for $\mu > \mu_c = 3$, where μ is the decay of the noise amplitude. The results indicate that augmentation of μ exponent and conspicuity of the Gaussian ballistic deposition model prepare to decrease the structure porosity and multi-affinity, and also increase the contour loop area and perimeter.

1 Introduction

To analyze roughness surfaces resulting from nonequilibrium growth phenomena, combining the approaches obtained from theoretical analysis and computational simulation is necessary to get the desired results. Fluctuations in rough surfaces obtained during growth are often characterized by discrete statistical models implemented in Monte Carlo algorithms [1,2]. Discrete significant and fundamental growth models include random deposition (RD) [3,4], ballistic deposition (BD) [5], random deposition with surface relaxation (RDSR) [6,7], and solid-on-solid [8]. Among these models, the ballistic deposition model belonging to the universality class Kardar-Parizi-Zhang (KPZ) has special features due to its porous structure and has received attention [9,10]. In a ballistic deposition model, particles that randomly land on a substrate can stick to neighboring particles on first contact, which causes a correlation between the accumulated particles and the creation of the porous structure. The size and shape of the particles, the size and shape of the pores created, and the orientation of the accumulated particles and pores can affect the thermal [11], electrical [12,13], and optical properties of the material [14].

The differential equation that denotes the variation of height, *h(x,t)*, with time, *t*, at any position *x* in a growth model is given by:

*Corresponding author.
Email address: K.Rahimi@Alzahra.ac.ir
DOI: 10.22051/jitl.2024.45106.1096

$$\frac{\partial h(x,\,t)}{\partial t} = F + \eta\,(x,\,t), \qquad (1)$$

where F is the average number of particles at site x and the noise $\eta(x, t)$ expresses the random fluctuations in deposition processes. In general mode the value of $\eta(x, t)$ is chosen as uncorrelated Gaussian distributed noise, but there are events that cannot be explained by a Gaussian noise [15,16]. For example, in the investigation of fluid flow in porous environments, a power-law distributed noise has been observed in which the noise amplitude follows a power law as follows [17]:

$$p(\eta) \approx \mu\eta^{-(\mu+1)}, \qquad (2)$$

where $\eta > 1$, while μ is an exponent that characterizes the decay of the noise amplitude. By decreasing the exponent μ, the uniformity of the power-law noise is reduced, and by increasing it, the power-law noise approaches the Gaussian one.

Random processes in nature can create fractal structures. The fractal analysis includes various techniques for allocating a fractal dimension and other fractal properties to a data set. This data set can be a pattern or signal from natural objects [18], ecology science [19], market fluctuations [20,21], digital images [22], and surfaces growth [23]. Analysis of fractal systems has been done using mathematical and numerical techniques in the development of fractional calculations [24,25]. In inspecting the complexity of structures that show how objects fill the available space, a criterion called the fractal dimension is used [26]. The fractal dimension can be used to understand the desired phenomenon. For example, rougher surfaces have a larger fractal dimension, and their fractal dimension can be calculated to estimate the roughness of the surface.

In investigating rough surfaces, it is observed in most cases that the surface growth is not isotropic in all directions and that such irregularities lead to multifractal behaviors [27,28,29]. This irregularity is not present in monofractal structures and, they are parameterized by a scaling exponent at all scales. Multifractal scaling analysis has been utilized in the review of growth models as the solid-on-solid model [30], diffusion-limited aggregation surfaces [31], and the random-deposition model [32].

Contour fractal analysis is another type of fractal analysis in which information is addressed from point to point of a surface. Contour loops are obtained by connecting points with the same height which are non-intersecting closed lines. Loops often have fractal properties related to the roughness and morphology of the underlying surfaces. Contour analysis of rough surfaces has been applied for Gaussian surfaces [33,34], KPZ surfaces [35], etched silicon rough surfaces [36], WO3 experimental rough surfaces [37], and random deformations of suspended graphene sheets [38].

In this paper, the ballistic deposition model with a power-law distributed noise (BD-PLN) has been simulated, and the contour fractal analysis and multifractal analysis have been investigated. Section *II* presents details of the generation of the rough surface, and in Sections *III* and *IV*, contour fractal analysis and the multifractal analysis are considered. Section *V* discusses the results, and finally in Section *V I* the conclusion will be given.

2 BD-PLN model

The two-dimensional BD-PLN model is made by landing and accumulating heterogeneous particles that land directly and vertically on a flat substrate. The particle position, x, is randomly selected. Falling particles are rod-like and their length, l, follows the power-law distribution of Eq. (2)

$$l = int\left(r^{-\frac{1}{\mu}}\right), \qquad (3)$$

where l is the rod length, r is a random number uniformly distributed over the interval (0,1), and μ indicates the decay of the noise amplitude chosen as $\mu \geq 1$. At a random position x, the landing particle sticks to its top or nearest neighbor particle and rises to a height of $h(x)$. The dynamic of this process is shown as follows:

$$h(x, t+1) = [\max(h(x-1, t), h(x, t) + 1, h(x, t+1))]. \qquad (4)$$

At $t = 0$ for all x, $h(x, t) = 0$, and periodic boundary conditions are applied at each time step to limit the sites in the expected range [1, L], where L is the size of the substrate. According to the Monte Carlo simulation, time steps equal to the size of the system, L, are considered. At each step, L particles are randomly

landed and accumulated. Figure 1 shows a schematic view of heterogeneous particle deposition in the BD-PLN model.

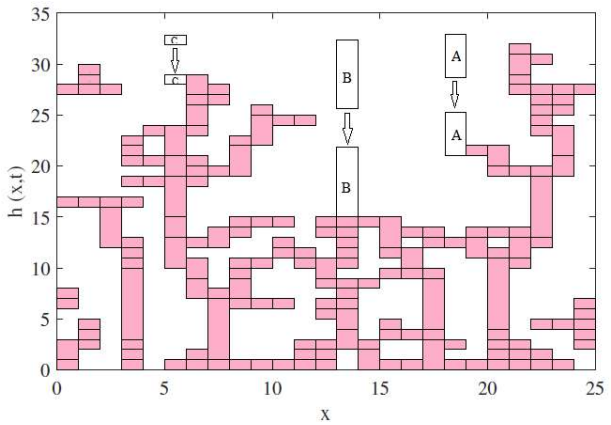

Figure 1. Schematic view of the accumulation of heterogeneous particles in the BD-PLN model. The particles (A, B, and C) vertically come down and stick to their top or nearest neighboring particles.

The Hoshen-Kopelman algorithm determines homogeneous patches in a 2D matrix. In this algorithm, the cluster size array is identified and labeled with the appropriate index. In each surface set of lines of equal height, for each loop, the length of the loop or its perimeter, s, can be defined as which has a radius of R length. The length of the loop is equal to the number of unit cells that make up the contour loop. The radius of a loop is calculated by the following equation:

$$R^2 = \frac{1}{N}\sum_{i=1}^{N}[(xi - xc)^2 + (yi - yc)^2], \quad (5)$$

where $xc = \frac{1}{N}\sum_{i=1}^{N} xi$ and $yc = \frac{1}{N}\sum_{i=1}^{N} yi$ are the central mass coordinates. By considering the scaling behavior of the averaged loop perimeter, $\langle s \rangle$, versus averaged loop radius, $\langle R \rangle$, the fractal dimension of each loop, D_f, is determined by the following:

$$\langle s \rangle \sim \langle R \rangle^{D_f}. \quad (6)$$

In order to calculate the fractal dimension of all the loops formed on the surface, the box-counting method has been used. The box-counting dimension is used by many researchers who work on fractal analysis due to the ease of calculations [40,41]. For scaled quantification with the box-counting method, the desired pattern is cut into smaller pieces, usually in the form of a square with the size r.

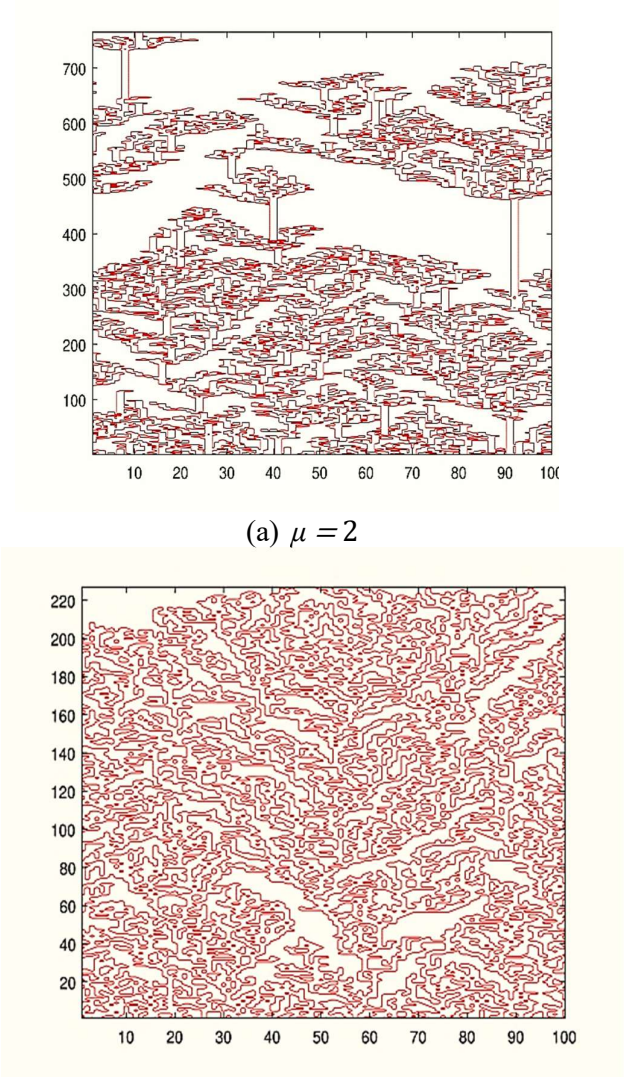

(a) $\mu = 2$

(b) $\mu = 6$

Figure 2. The contour lines created in the side-view of the BD-PLN model for different values of μ,

The number of boxes covering the shape is changed by taking boxes with different side lengths. As the side length decreases toward zero, the boxes tend to cover the real fractal more. The side-view images of the BD-PLN model with different μ values were derived. The boxes that cover the fractal loops are counted as $N(r)$. The scale relation between $N(r)$ and r is:

$$N(r) \sim r^{-d}. \quad (7)$$

where d is the fractal dimension of all loops located in the side-view of the BD-PLN model.

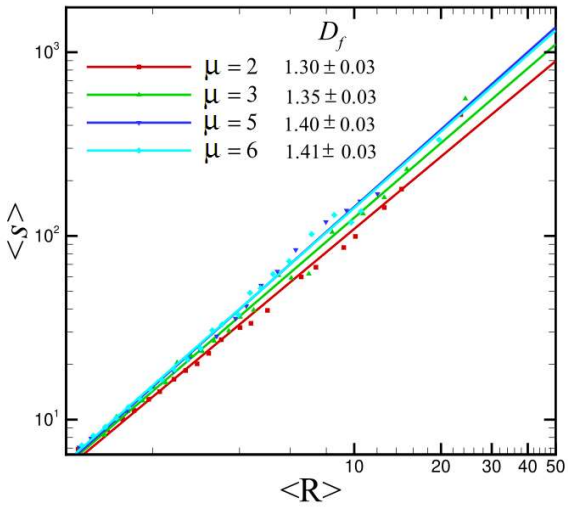

Figure 3. The log-log diagram shows ⟨s⟩, versus ⟨R⟩ for different values of μ.

4 Multifractal Analysis

Different methods to detect multi-affinity in complex systems have been introduced, such as spectral analysis [42], fluctuation analysis [43], wavelet transform module maxima [44], and multifractal analysis [45,46]. The fractal dimension obtained from the box-counting method ignores irregularities smaller than the size of r. Therefore, the number of points found in the boxes that cover the shape are not proportional to each other. To investigate any irregularity in the resulting porous structures of the BD-PLN model, multifractal analysis is implemented. The multifractal dimension is defined by the following equations:

$$D_q = \frac{1}{q\text{-}1}\tau_q \quad \text{for} \quad q \neq 1, \tag{8}$$

$$\tau_q = lim_{r\to 0}\frac{log\ Zr,q}{-log\ r}, \tag{9}$$

$$Z_{r,q} = \sum_i (z_{i,r})^q \approx r^{(1-q)D_q} \approx r^{\tau_q}, \tag{10}$$

where D_q is the generalized dimensions, τ_q is the mass function, which is used to determine the behavior of the system, $Z_{r,q}$ is the structure-function, and $z_{i,r}$ measures the proportion of occupied cells in the grid box i of size r. The parameter, q, belongs to the set of real numbers, and in this research, its changes is arbitrarily chosen in the range of (-5, +5). The value of D_q is determined by the changes of q in this interval. $D(q = 0)$ describes the capacity dimension, which is candid for the box-counting dimension, $D(q = 1)$ is equal to the information dimension, and $D(q = 2)$ displays the correlation dimension. In multifractal analysis, there are multiple dimensions in the D_q versus q ranges, but monofractals dwell pretty flat in that area. The next section, discusses these parameters and fractal features of the BD-PLN model.

5 Results and discussion

As discussed in Sec. *II*, the rod-like particles with variable lengths are deposited using the Monte Carlo algorithm in the ballistic deposition model. The length of particles follows from a power-law distribution, $p\ (l) \sim \mu\ l^{-(\mu+1)}$, and as in Fig. 1 has been shown, the deposition of particles in the ballistic deposition model has led to the formation of a porous structure. To draw the contour loops, the BD-PLN model for different exponents μ was simulated, and by employing the Hoshen-Kopelman algorithm [39], contour loops were generated (Fig. 2). As in Fig. 2 has been depicted, the change of μ has an affection on the shape of the contour loops, when μ decreases, the space between the contour loops increases, and the tendency to stretch the loops in the vertical direction increases.

To calculate the fractal dimension of a contour loop, the pyramid and radius of gyration of different loops are checked under the influence of power-law noise. The fractal dimension of each loop, D_f, is identified by the logarithmic scaling of the average pyramid of the loop, ⟨s⟩ , versus of the averaged loop radius, ⟨R⟩ (Fig. 3). The slopes of Fig. 3 show that the fractal complexity of the loop rises with increasing μ. The following power equation is obtained by drawing D_f versus μ in Fig. 4 and using the Table Curve Software,

$$D_f = \mu^b. \tag{11}$$

where a= 1.21± 0.01 and b= 0.09± 0.01.

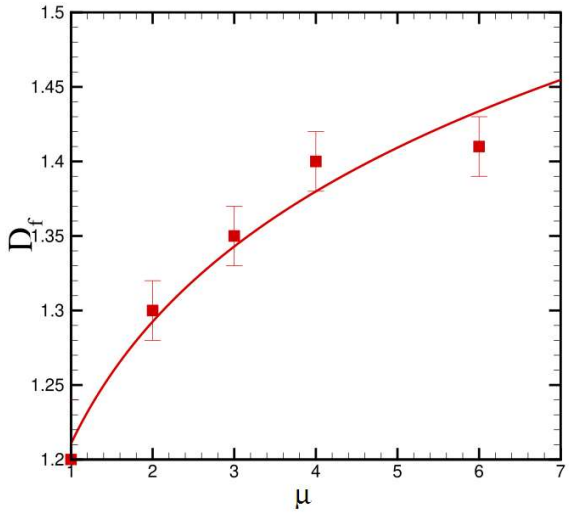

Figure 4. The dimension, D_f, respect to the μ exponent.

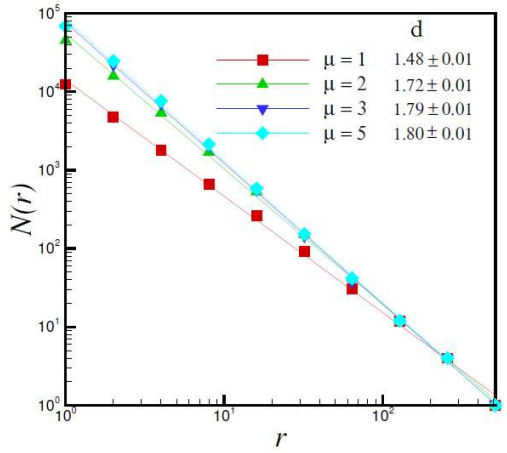

Figure 5. The log-log diagram of the number of boxes, *N(r)*, versus the box sizes, *r*.

To show the fractal complexity of the side-view of the BD-PLN model during the growth process, the fractal dimension of all loops by using the box-counting method is obtained. The log-log plot of the number of boxes, *N(r)*, versus the size of the boxes, *r*, is depicted in Fig. 5. The fractal dimension of all loops in Gaussian noise is single-valued, but this stability is not observed in power-law noise. As shown in Fig. 5, by changing the values of μ, different slopes are obtained for the fractal dimension, *d*. The obtained relationship between the dimension, *d*, and the μ exponent is as the following equation:

$$d = a + b\mu^c. \quad (12)$$

where a = 1.82 ± 0.01, b = -0.34 ± 0.01, and c= -1.8 ± 0.2. Also as depicted in Fig. 6, the fractal dimension increases and is saturated at $\mu > \mu_c = 3$, and picks up a constant value, $d = 1.80 \pm 0.01$. The point $\mu_c = 3$ indicates the position where the power-law noise changes to a Gaussian one.

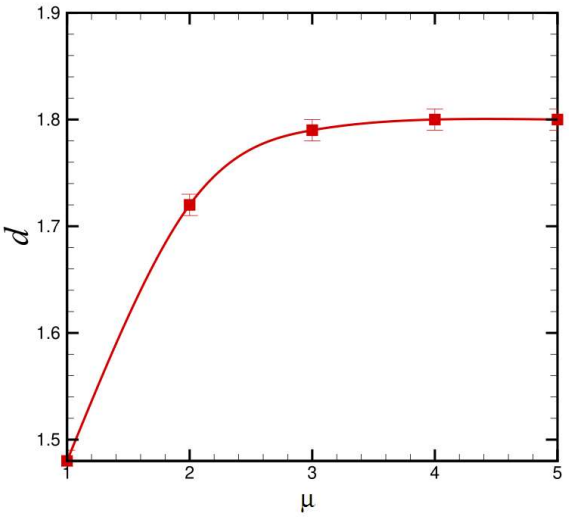

Figure 6. The dimension, *d*, respect to the μ exponent.

The multifractal analysis is also performed to investigate the irregularity in the porous structure of the BD-PLN model. Before this, multifractal analysis has been done for the random deposition model with the power law noise, (RD-PLN) model, and the multiaffinity behavior for the height fluctuations with $\mu < \mu_c$ has been observed [47]. As discussed in Sec. III., the fractal dimension obtained from the box-counting method does not show local irregularities and only conveys the average information of the network. So to describe the mass changes with box size, r, in an image, and its behavior when the image was scaled or cropped and distorted by q value, the D_q parameter is used. As illustrated in Fig. 7 the generalized dimensions are plotted versus q for different values of μ. For distorting the data set, the arbitrary value of q is chosen in the range of (-5, +5). Normally, the value of the symmetric interval q is taken to have the value of zero, which corresponds to the box-counting dimension, in the bracket. It has been considered that by taking the range of q wider and wider the measurement error caused by the large volume of measurement data is added, and could affect the multifractal spectrum [48].

Figure 7 indicates that the non-linear state of the graph decreases with the increase of μ and converges to a certain value, which indicates the monofractal state and the emergence of Gaussian noise. While in $\mu \leq \mu_c = 3$, where the length of stacked rods is longer, a humped state is observed. This non-linear mode revealed the multi-affinity of the growth structure in $\mu \leq \mu_c = 3$ and the appearance of multifractal properties.

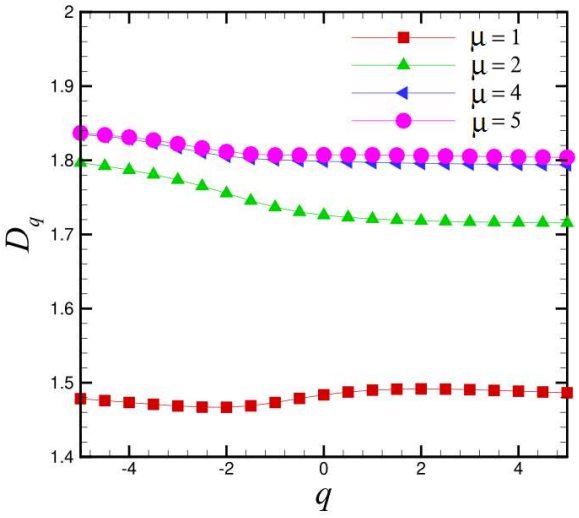

Figure 7. The generalized dimensions, D_q, for different values of μ exponents.

The mass exponent, τ_q, is used to determine the behavior pattern of the system. Figure 8 shows the τ_q vs. q for different values of μ exponents. As shown in Fig. 8, for q = 0, $\tau_{(q=0)} = -D_{(q=0)}$, where $D_{(q=0)}$ is the dimension of the box-counting method. Also the normalization of Eq. (10) leads to for q = 1, $\tau_{(q=1)} = 0$, and for a complete uniform distribution, τ_q is obtained by using Eq. (8), $D_q = \frac{1}{q-1}\tau_q$. So the slopes of curves in Fig. 8 get a linear form for $\mu > \mu_c = 3$, where the Gaussian noise appears and the generalized dimension, D_q, reaches a constant value. On the contrary, the nonlinearity of the graph in Fig. 8 for $\mu \leq \mu_c = 3$ shows the tendency of the structure to a multifractal pattern. Also, research has shown that the non-linearity of τ_q vs. q has led to an increase in the distribution range of the singularity spectrum of fractals, which is used to show the strength of the irregularities of the measure [49].

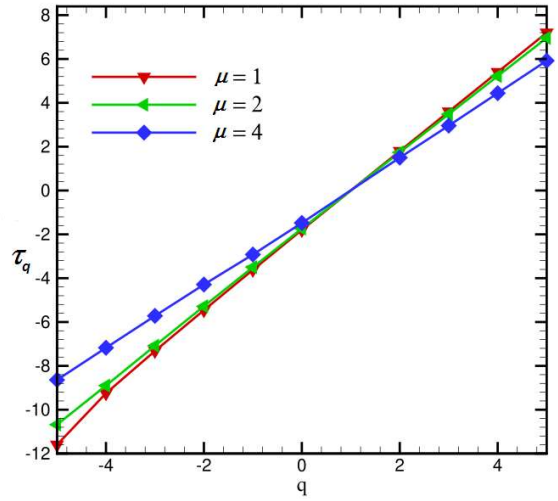

Figure 8. The mass function, τ_q versus q for different values of μ exponents.

6 Conclusions

The contour loops in the BD-PLN model by using Monte Carlo and Hoshen-Kopelman algorithms have been simulated. In the BD-PLN model, rod-like particles with variant lengths were deposited, and the length of the particles was determined by a power-law distribution, $p(l) \sim \mu l^{-(\mu+1)}$. Using geometrical exponents including the fractal dimension of each loop, the fractal dimension of all loops in the contour set, and the multifractal dimension can characterize the complexity and morphology of porous structures. The results displayed that for $\mu \leq \mu_c = 3$ where the length of rods was long, the porosity of the structure was enhanced, the fractal dimension of each loop, and the fractal dimension of the contour set decreased. Also, the relationship between these dimensions with the μ exponent was formulated. In the following, the multifractal scaling analysis was performed and was shown that the multi-affinity strength increased, while the power-law noise dominated Gaussian noise, led to nonlinearity form in generalized dimension and mass exponent. Future research endeavors in the field of studying the geometrical exponents of contour loops on the ballistic deposition model with power-law distributed noise could lead to new perspectives and advancements, new avenues to explore and new questions to answer.

References

[1] T. Shitara, D. D. Vvedensky, M. R. Wilby, J. Zhang, J. H. Neave, and B. A. Joyce, "Step-density variations and reflection high-energy electron-diffraction intensity oscillations during epitaxial growth on vicinal GaAs(001)." Physical Review B, **46** (1992) 6815.

[2] J. W. Evans, P. A. Thiel, and M. C. Bartelt, "Morphological evolution during epitaxial thin film growth: Formation of 2D islands and 3D mounds." Surface Science Report, **61** (2006) 1.

[3] D. A. Mirabella and C. M. Aldao, "Surface growth by random deposition of rigid and wetting clusters." Surface Science, **646** (2016) 282-287.

[4] F. L. Forgerini and W. Figueiredo, "Random deposition of particles of different sizes." Physical Review E, **79** (2009) 041602.

[5] Y. Pellegrini and R. Jullien, "Ballistic deposition of clusters." Physica A: Statistical Mechanics and its Applications, **165** (1990) 19-30.

[6] R. C. Buceta, D. Hansmann, and B. von Haeften, "Revisiting random deposition with surface relaxation: approaches from growth rules to the Edwards-Wilkinson equation." Journal of Statistical Mechanics: Theory and Experiment, **2014** (2014) 12028.

[7] S. Hosseinabadi, Z. Karimi, and A. A. Masoudi, "Random deposition with surface relaxation model accompanied by long-range correlated noise." Physica A: Statistical Mechanics and its Applications, **560** (2020) 125130.

[8] S. Hosseinabadi, A. A. Masoudi, and M. S. Movahed, "Solid-on-solid model for surface growth in 2+1 dimensions." Physica B: Condensed Matter, **405** (2010) 8.

[9] H. F. El-Nashar, W. Wang, and H. A. Cerdeira, "Surface growth kinetics and morphological structural transition in a (2 + 1)-dimensional deposition model." Journal of Physics Condensed Matter, **8** (1996) 3271.

[10] S. K. Das, D. Banerjee, and J. N. Roy, "Particle Shape-Induced Correlation Effect in Random Deposition in 1+1 Dimension and Related Effect in Ballistic Deposition." Surface Review and Letters, **28** (2021) 2050043.

[11] I. Sumirat, Y. Ando, and S. Shimamura, "Theoretical consideration of the effect of porosity on thermal conductivity of porous materials." Journal of Porous Materials, **13** (2006) 439–443.

[12] R. Dasgupta, S. Roy, and S. Tarafdar, "Correlation between porosity, conductivity and permeability of sedimentary rocks |a ballistic deposition model." Physical Review A, **275** (2000) 22-32.

[13] Z. Ebrahiminejad, H. Hamzehpour, and S. F. Masoud, "Electrical conductivity of thin films grown by deposition of random clusters of particles." Journal of Material Science: Materials in Electronics, **27** (2020) 1-10.

[14] A. Mortezaali, S. Ramezani Sani, and F. Javani Jooni, "Correlation Between Porosity of Porous Silicon and Optoelectronic Properties." Journal of Non-Oxide Glasses, **1** (2009) 293 – 299.

[15] J. M. Kim and H. Choi, "Depinning Transition of the Quenched Edwards-Wilkinson Equation." Journal of the Korean Physical Society, **48** (2006) 241-244.

[16] S. Hosseinabadi and A. A. Masoudi, "Random deposition with a power-law noise model: Multiaffine analysis." Physical Review E, **99** (2019) 012130.

[17] M. A. Rubio, C. A. Edwards, A. Dougherty, and J. P. Gollub, "Self-affine fractal interfaces from immiscible displacement in porous media." Physical Review Letters, **63** (1989) 1685.

[18] F. Gerges, X. Geng, H. Nassif, and M. Boufadel, "Anisotropic Multifractal Scaling of Mount Lebanon Topography: Approximate Conditioning." Fractals, **29** (2021) 2150112.

[19] S. Laurent, "Fractals and Multifractals in Ecology and Aquatic Science." CRC Press, 2009, Ch. 7.

[20] R. Mulligan, "Fractal analysis of highly volatile markets: an application to technology equities." The Quarterly Review of Economics and

Finance, Elsevier, **44** (2004)155–179.

[21] S. Kamenshchikov, "Transport Catastrophe Analysis as an Alternative to a Monofractal Description: Theory and Application to Financial Crisis Time Series." Journal of Chaos, **2014** (2014) 346743.

[22] F. Zappasodi, E. Olejarczyk, L. Marzetti, and G. Assenza, "Fractal Dimension of EEG Activity Senses Neuronal Impairment in Acute Stroke." PLOS ONE, **9** (2014) 100199.

[23] E. E. Mozo Luis, F. A. Oliveira, and T. A. de Assis, "Accessibility of the surface fractal dimension during film growth." Physical Review E, **107**, (2023) 034802.

[24] S. Qureshi, M. A. Akanbi, A. A. Shaikh, A. S. Wusu, O. M. Ogunlaran, W. Mahmoud, and M. S. Osman, "A new adaptive nonlinear numerical method for singular and stiff differential problems." Alexandria Engineering Journal, **74** (2023) 585-597.

[25] A. Padder, L. Almutairi, S. Qureshi, A. Soomro, A. Afroz, E. Hincal, and A.Tassaddiq, "Dynamical Analysis of Generalized Tumor Model with Caputo Fractional-Order Derivative." fractal and fractional, **7** (2023) 7030258.

[26] B. B. Mandelbrot, "The fractal geometry of nature.", Echo Point Books and Media, LLC., 2021, ch. 2.

[27] D. Sornette, "Critical Phenomena in Natural Sciences." Chaos, Fractals, Self-organization and Disorder: Concepts and Tools Springer-Verlag, Heidelberg, 2000, 123-160.

[28] S. Hosseinabadi, M. A. Rajabpour, M. Sadegh Movahed, and S. M. Vaez Allaei, "Geometrical exponents of contour loops on synthetic multifractal rough surfaces: Multiplicative hierarchical cascade p model." Physical Review E, **85** (2012) 031113.

[29] S. Hosseinabadi and M. Rajabi, "Roughness kinetic and multiaffinity of anisotropic etched silicon." Superlattices and Microstructures, **102** (2017) 180-188.

[30] W. Bing, W. Yan, and W. Ziqin, "Multifractal behavior of solid-on-solid growth." Solid State Communications, **96** (1995) 69-72.

[31] W. G. Hanan and D. M. Heffernan, "Multifractal analysis of the branch structure of diffusion-limited aggregates." Physical Review E, **85** (2012) 021407.

[32] A. Chaudhari, C. C. S. Yan, and S. L. Lee, "Multifractal analysis of growing surfaces." Applied Surface Science, **238** (2004) 513-517.

[33] S. Hosseinabadi, S. M. S. Movahed, M. A. Rajabpour, and S. M. V. Allaei, "Dynamical and geometrical exponents of self-affine rough surfaces on regular and random lattices." Journal of Statistical Mechanics: Theory and Experiment, **12** (2014) 12023.

[34] J. Kondev, and C. L. Henley, "Geometrical Exponents of Contour Loops on Random Gaussian Surfaces." Physical Review Letters, **74** (1995) 4580.

[35] A. A. Saberi, M. D. Niry, S. M. Fazeli, M. R. Rahimi Tabar, and S. Rouhani, "Conformal invariance of isoheight lines in a two-dimensional Kardar-Parisi-Zhang surface." Physical Review E, **77** (2008) 051607.

[36] S. Hosseinabadi, "Iso-height lines of multifractal etched silicon rough surfaces." Materials Science in Semiconductor Processing, **88** (2018) 79–85.

[37] M. A. Rajabpour, and S. M. Vaez Allaei, "Scaling relations for contour lines of rough surfaces." Physical Review E, **80** (2009) 011115.

[38] I. Giordanelli, N. Posé, M. Mendoza, and H. J. Herrmann, "Conformal Invariance of Graphene Sheets." Scientific Reports, **6** (2016) 22949.

[39] J. Hoshen and R. Kopelman, "Percolation and cluster distribution. I. Cluster multiple labeling technique and critical concentration algorithm." Physical Review B, **14** (1976) 3438.

[40] M. Bouda, J. S. Caplan, and J. E. Saiers, "Box-Counting Dimension Revisited: Presenting an Efficient Method of Minimizing Quantization

Error and an Assessment of the Self-Similarity of Structural Root Systems." Frontiers in Plant Science, Sec. Technical Advances in Plant Science, **7** (2016) 149.

[41] J. Z. Liu, L. D. Zhang, and Y. H. Guang, "Fractal Dimension in Human Cerebellum Measured by Magnetic Resonance Imaging." Biophysical Journal, **85** (2003) 4041-4046.

[42] T. Babadagli and K. Develi, "On the application of methods used to calculate the fractal dimension of fracture surfaces." Fractals, **9** (2001) 105-128.

[43] C. K. Peng, S. Buldyrev, A. Goldberger, S. Havlin, F. Sciortino, M. Simons, and H. E. Stanley, "Long-range correlations in nucleotide sequences." Nature (London), **356** (1992) 168-170.

[44] Z. R. Struzik, and A. P. J. M. Siebes, "Wavelet transform based multifractal formalism in outlier detection and localisation for financial time series." Physica A, **309** (2002) 388.

[45] J. Zhang, C. Wei, X. Chu, V. Vandeginste, and W. Ju, "Classification of Pore–fracture Combination Types in Tectonic Coal Based on Mercury Intrusion Porosimetry and Nuclear Magnetic Resonance." ACS Omega, **5** (2020) 19385-19401.

[46] A. Dathe, A. M. Tarquis, and E. Perrier, "Multifractal analysis of the pore- and solid-phases in binary two-dimensional images of natural porous structures." Geoderma, **134** (2006) 318–326.

[47] S. Hosseinabadi and A. A. Masoudi, "Random deposition with a power-law noise model: Multiaffine analysis." Physical Review E, **99** (2019) 012130.

[48] H. Chen, X. Sun, H. Chen, Z. Wu, and B. Wang, "Some problems in multifractal spectrum computation using a statistical method." New Journal of Physics, **6** (2004) 84.

[49] A. Chaudhari, C. C. Sanders Yan and S. L. Lee, "Eley–Rideal diffusion limited reactions over rough surface." Physical Chemistry Chemical Physics, **4** (2002) 5330–5334.